A Dispersed Anisotropic Phase as the Origin of the Weak-Gel Properties of Aqueous Xanthan Gum

J. O. CARNALI

Unilever Research U.S., Inc., 45 River Road, Edgewater, New Jersey 07020

SYNOPSIS

Xanthan gum is a water-soluble, extracellular polysaccharide that has gained widespread commercial use because of its strong pseudoplasticity and tolerance to high ionic strength. It possesses a rigid, rodlike structure and has been reported to form weak gels at concentrations on the order of 0.5%. The nature of these weak gels has been explored using creep measurements and dynamic mechanical spectroscopy. The usual weak gel symptoms are found in 0.02N KCl at xanthan levels exceeding 0.8% and include deviations from the Cox–Merz rule ($\eta^* > \eta$), onset of weak power-law dependence of the loss and storage moduli, and appearance of unusually long relaxation times. We have also detected an apparent yield stress for concentrations beyond 0.8%. However, concentration-independent relaxation times and a slip/stick behavior during extended flow runs also marked the weak gel region and suggested sample heterogeneity. This condition was confirmed by optical studies that showed samples in this region to consist of a nematic liquid crystalline phase dispersed in an isotropic phase. The conclusion is made that the unusual rheological behavior of xanthan can be traced to the occurrence of this phase separation. Possible mechanisms for the formation of the anisotropic phase are also discussed.

INTRODUCTION

From its development less than 30 years ago,[1] xanthan gum has become a widely used structurant in all areas of technology.[2] It is highly prized for its strong pseudoplasticity in aqueous solution and for its tolerance of high ionic strengths.[3–5] Xanthan gum is an extracellular polysaccharide based upon a β-1,4-linked glucan backbone as in cellulose.[6,7] It possesses a polyelectrolyte character due to every second glucose residue carrying a charged trisaccharide side chain. The conformation of this biopolymer is fascinatingly varied with an order (helix)-to-disorder (coil) transition occurring upon heating. Possibilities suggested for the low-temperature structure have included an intramolecular helix stabilized by noncovalent side-chain/main-chain interactions. These interactions lead to an ordered packing of the side chains along the polymer backbone to give the fundamental ordered structure.[8] A second proposed structure for xanthan consisted of a multistranded stack of up to 40 component single chains.[9] The driving force for this agglomeration could be the same forces as mentioned above but may also involve hydrophobic interactions between pyruvate-substituted side chains.[10] The model currently accepted by the majority of workers is a double chain occurring as a helix or as a side-by-side agglomerate.[11] The stability of this ordered conformation is extended to higher temperatures at increasing ionic strength.

The helical form of xanthan acts as one of the stiffest rod-shaped molecules known. With a molecular weight of $1–3 \times 10^6$, xanthan has a Kratky–Porod persistence length of 100–300 nm (Ref. 12) or over 10 times that of sodium carboxymethylcellulose and comparable to that of DNA.[12,13] With a mass per unit length of 1000–2000 daltons/nm, it can be thought of as a semirigid rod with an aspect ratio in the range 250–500 (1000 nm in length, 2–4 nm in diameter).[2,14,15]

Its molecular conformation alone, however, is not the explanation for the interesting rheological behavior exhibited by xanthan gum. Unique, "gel-like"

Journal of Applied Polymer Science, Vol. 43, 929–941 (1991)
 CCC 0021-8995/91/050929-13$04.00

properties have long been noted in xanthan solutions of moderate concentration.[2,6,16] Typical values for the overlap concentration, c^* ($\sim 1/[\eta]$), range from 0.02% to 0.04% (Refs. 12–14, 17), and the weak gel behavior is typically first noted by 0.5% ($c[\eta] \sim 15$). Such systems are barely into the concentrated regime[18] and would be expected to just be beginning to show the effects of entanglement coupling.[8] Instead, such systems display stronger shear thinning behavior than is typically found in even profoundly entangled networks[3,18] with the shear thinning index (n in $d \log \eta / d \log \gamma' = n - 1$) being typically around 0.1. There is, further, no evidence of the usual Newtonian plateau in the shear viscosity at low shear rates,[8,19] though such plateaus are evident at concentrations below 0.5%.[2,15,20] Mechanical spectroscopy reveals that the elastic modulus (G') exceeds the loss modulus (G'') throughout the typical experimental frequency range (10^{-2}–10^2 rad/s) and that the frequency dependence is rather weak.[14] The Cox–Merz rule is found to be disobeyed with the complex viscosity [$\eta^*(\omega)$] exceeding the shear viscosity ($\eta(\gamma')$).[6,7,19]

There is at the moment some controversy as to whether or not xanthan solutions possess a yield stress and if they can be classified as gels. Original claims of yield stresses at 1% xanthan[2] were refuted[14,19] based upon the shear thinning index being distinctly nonzero and the absence of a low-frequency plateau in G'. Now, fresh evidence indicates that some xanthans can form gels at only 0.22% levels.[15] It is clear that these conflicting reports stem from differences in gum samples and in the means of analysis. Gels, if formed at all with xanthan, are thought to belong to the class of weak gels[8,21] in which the intermolecular interactions that lead to physical cross-linking are reversible on the time scale of the experiment. These intermolecular interactions are in excess of chain entanglements and, for the case of xanthan, may include hydrogen-bonding, cation-mediated, and hydrophobic effects.[6,7,10,13]

In addition to a microstructure consisting of randomly oriented rods with attractive interactions, other models have been proposed for the "weak gel" phase of xanthan. One possible explanation is that it is due to aggregates of xanthan molecules called microgel particles. These aggregates could result from the above intermolecular interactions or arise as an artifact of the drying process[22] used to isolate the gum. The net result is that the xanthan solution actually consists of a dispersion of particles.[9,23] Further interaction between these particles could lead to a disordered network array. Evidence for microgel formation comes from light scattering (nonexponential decay of the correlation function combined with long correlation times)[9,15] and from viscosity measurements (presence of a yield stress and long filtration times).[15] The microgel can be "melted" to some extent by thermal treatment[15,23] or degraded and removed by centrifugation and ultrafiltration.[13] However, slow reaggregation is observed that gradually restores the symptoms in light scattering and viscosity studies.[7,23]

A closely related explanation[8,13] hinges on the known fact that concentrated (> 1%) solutions of rod-shaped particles such as xanthan can increase their entropy by forming an anisotropic phase in which the rods are oriented parallel to one another. At certain compositions, a two-phase system could result, consisting of a dispersion of anisotropic phase within isotropic phase.[14] Such dispersions would dominate rheological properties by imparting nonlinearities in dynamic measurements and causing long relaxation times.

The original goal of the work described below was to study the gelation point in xanthan solutions. Recent work by Winter et al.[24,25] has indicated that chemically cross-linked gels display universal rheological properties at the gel point. It was thought that if gelation could be detected in xanthan systems, there might be an opportunity to test Winter's predictions on a highly nonideal, physically cross-linked system. Since the xanthan gels were expected to be weak, controlled stress techniques were employed that allow characterization at very low shear rates and over very long time scales. Further, gum concentration was chosen as the means with which to approach gelation since this is the natural variable in systems of this kind. Convincing evidence for formation of a weak gel was found in this system, but physical cross-links between polymer chains does not appear to be the cause. Rather, our findings indicate that the unique "gel-like" properties of xanthan are due to the biphasic nature of its concentrated solutions.

EXPERIMENTAL

The xanthan gum was a specially clarified commercial grade (Keltrol T) from Kelco that was determined to be 88% solids. The molecular weight of this material was determined as 4×10^6 by intrinsic viscosity measurements using the Mark–Houwink relation developed by Tinland and Rinaudo.[12] In 0.02N KCl, we have used

$$[\eta] = 3.45 \times 10^{-5} M^{1.24} \quad (1)$$

where the parameters are linearly interpolated from the data presented by the above authors. A Cannon–Ubbelhode four-bulb shear dilution viscometer was employed, and the log of the viscosity was extrapolated to zero shear rate to determine the limiting viscosity.[26] Centrifugation of a 0.2% dispersion of this material at 50,000g for 1 h gave no sediment, indicating negligible cell debris. Unless otherwise noted, this material was used without further purification to prepare aqueous dispersions. A small batch of purified xanthan was prepared by a procedure modified from that used by Holzwarth.[27,28] The biopolymer was precipitated from aqueous solution with ethanol, dialyzed against 0.1N KCl, exhaustively dialyzed against distilled water, and then lyophilized. Samples were prepared on a weight percent basis by dissolving the xanthan in 0.02M KCl (to maintain a concentration-independent conformation)[6–8] at room temperature with stirring. Dissolution times ranged from minutes at 0.3% xanthan up to days for the most concentrated (3%) sample. Samples were stored at 5°C and were used for a maximum period of 2 weeks before being discarded. Under these storage conditions, samples typically lasted 1 month before bacterial contamination could be detected. Gentle centrifugation was routinely used to remove air bubbles prior to measurements.

Rheological evaluation was performed using a Carrimed controlled stress rheometer (CS100) with a cone and plate (2°; 2 and 3 cm radius cone) or a concentric cylinder (0.75 mm gap, 2 cm bob radius) geometry. A solvent trap using distilled water was used to retard evaporative losses from the sample in the cone and plate geometry while a thin layer of 10 cP silicone oil over the annular gap accomplished the same task with the concentric cylinder. Since loading the sample into the rheometer gap necessarily involves fairly severe material deformation, equilibration times of 1–15 h were employed after loading before measurements were begun. A check was made to ensure that equilibration time did not affect the results.

Both creep and dynamic mechanical spectroscopy were employed to characterize the samples. In creep measurements, a series of stresses ranging up from 0.08 Pa were applied to the sample and its deformation followed with time until zero or steady flow was achieved. When extracting viscoelastic data from the creep curves, samples were allowed to recover, before the next increment in stress, for a period at least as long as that in which the stress had been applied. Creep curves were then fit according to the usual formula[29]:

$$J(t) = \gamma(t)/\sigma = J_g + \sum_i J_i(1 - \exp(-t/\tau_i)) + t/\eta \quad (2)$$

where $J(t)$ is the creep compliance defined as the strain divided by the applied stress, J_g is the "instantaneous" compliance, and η is the steady shear viscosity, and the summation term gives the retarded compliance. This latter term consists of a series of discrete contributions (J_i) to the compliance with corresponding retardation times τ_i.[29,30]

In oscillatory shear, a controlled stress loop in the Carrimed software was employed to give a frequency variation of 0.001–10 Hz (except for the concentric cylinder geometry where inertia corrections limited the upper range to 1 Hz). The strain amplitude was held constant during the sweep by the stress loop software, and strain levels of 20–40% were used as appropriate to keep within the material's linear viscoelastic range. The sample temperature was chosen at 25°C for all our work.

For measurement of the depolarized light intensity, a Hewlett Packard 8451A diode array spectrophotometer was modified by mounting sheets of polarized film just in front and behind the sample cell holder. The polarization axes of the sheets were set perpendicular to one another so that only depolarized light was detected by the photomultiplier tube. Measured intensity was referenced against the light transmitted through distilled water with only the first filter in place. Depolarized intensities were further corrected for the absorbance of the sample.

In the temperature-variation studies, samples were sealed in glass ampules and immersed within a thermostated glass beaker. Equilibration times of at least 1 h were employed, and sample birefringence was determined by mounting crossed polarized sheets before and after the beaker and then observing the transmitted light from a high-intensity lamp.

RESULTS

Oscillatory runs on xanthan samples with concentrations of 0.3, 0.4, 0.5, 0.6, 0.8, 1.0, 1.5, and 3% by weight were conducted, at least in duplicate, and found to be quite reproducible. The results are presented in terms of the storage modulus (G') and the loss modulus (G''), the complex viscosity ($\eta^* = (G'^2 + G''^2)^{1/2}/\omega$), and tan δ ($= G''/G'$, δ = loss angle) as functions of the angular frequency ω. Figure 1(a)

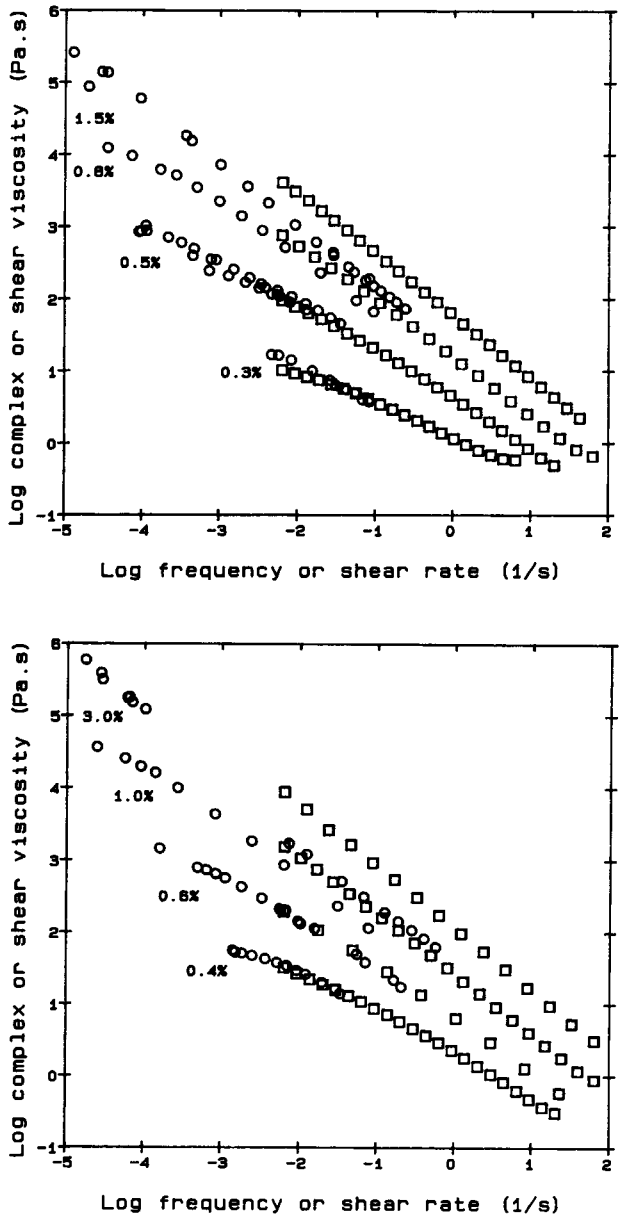

Figure 1 (a, b) Variation of the complex (square symbols) and shear (circle symbols) viscosities with frequency or shear rate, respectively, for a range of xanthan concentrations.

and (b) display η^* versus ω for all of the samples studied. In the log–log representation, the data are clearly representative of power-law fluids with η^* varying as ω^{n-1}, where n is the shear thinning index. The log η^*, log ω traces are strictly linear for xanthan concentrations over 0.8%. Below this concentration, some decrease in slope is evident at lower frequencies. Such behavior is expected for xanthan[3] and the "strength" of the pseudoplasticity, as indicated by the smallness of n, is reported in Table I. The shear thinning index clearly decreases with increasing biopolymer concentration, reaching a limiting value of about 0.14. This limit is comparable to that found by Santore and Prud'homme[19] for 4.7% xanthan in the absence of added electrolyte.

Figures 2 and 3 display G' and G'', respectively, versus frequency for the xanthan concentrations studied. It is clear that $G' > G''$ for the higher concentrations, so that these samples display dominating elasticity at small strains. The G' trace for concentrations of 0.8% and over follow a weak power law in frequency as recorded in Table I. This weak frequency dependence is usually interpreted as evidence for the weak gel nature of xanthan solutions with an intermolecular interaction occurring on very long time scales,[6,7] whereas the nonzero slope of G' is taken as indicating the absence of a true yield stress.[14] G'' shows similar power-law properties beyond 0.8%, but the slopes of the curves are slightly smaller than for G' (Table I). Thus, as shown in Figure 4, the linear trace of tan δ versus ω slopes downward for the higher concentrations. Concentrations below 0.8% display more "liquid-like" G', G'' traces with $G'' > G'$ at low frequencies as has been observed previously.[7] Consequently, tan δ exceeds 1 in Figure 4 for the 0.3% sample and the G'–G'' crossover is observed in Figure 5 to not occur until about 0.3 s^{-1}. As concentration increases, the crossover occurs at earlier frequencies: 0.1 s^{-1} for 0.4%, 0.02 s^{-1} for 0.5%, and below 0.006 s^{-1} for higher concentrations. Also shown in Figure 5 are the expected slopes for G' ($\sim \omega^2$) and G'' ($\sim \omega$) predicted at low frequencies and for G' and G'' ($\sim \omega^{1/2}$) predicted at high frequencies by the Rouse model for linear, flexible chains. The xanthan data clearly do not extend to low enough frequencies to determine conclusively whether or not the Rouse limit is obeyed. The trend at high frequency is toward a weaker dependency than the Rouse or the Zimm models would predict.[18]

Figure 1 (a) and (b) also display the steady shear viscosities, η, extracted from the creep results according to eq. (2). By doing creep measurements at a series of increasing stress levels, flow curves were generated over a shear rate (γ') range that extended down as far as 10^{-5} s^{-1}. For xanthan concentrations of 0.6% and under, the traces of log η versus log γ' superimpose nicely on the log η^* versus log ω data as prescribed by the Cox–Merz rule. The data further continue the dynamic flow curves to lower shear rates, hinting that a zero-shear, limiting viscosity plateau may exist for the 0.3 and 0.4% systems as has previously been observed by Chauveteau[20] and by Whitcomb and Macosko[2] for equivalent concentrations. These results are in keeping with the G',

Table I Shear Thinning Indices for G', G'', and η^*, η Over a Range of Xanthan Concentrations Along with the Limiting Compliances (J_{lim}) and Yield Stresses (τ_Y)

Xanthan Concentration (wt %)	$n_{G'}$	$n_{G''}$	$n_{\eta^*,\eta}$	J_{lim} (Pa^{-1})	τ_Y (Pa)
0.5	—	—	0.35[a]	—	—
0.6	—	—	0.30	—	—
0.8	0.25[b]	0.13[c]	0.25	0.7 ± 0.1	0.3 ± 0.1
1.0	0.20	0.10	0.18	0.6 ± 0.15	0.9 ± 0.2
1.2	—	—	—	0.3 ± 0.1	1.4 ± 0.2
1.5	0.15	0.05	0.14	0.09 ± 0.01	3.5 ± 0.3
3.0	0.13	0.07	0.14	0.05 ± 0.01	10.0 ± 1

[a] $\eta^* \sim \omega^{n-1}$, $\eta \sim \gamma'^{n-1}$.
[b] $G' \sim \omega^n$.
[c] $G'' \sim \omega^n$.

G'' traces that show "dilute" xanthan to behave as a typical polymer solution for which a viscosity plateau should occur. At 0.5 and 0.6%, no hint of a limiting viscosity is given. Rather, the shear thinning trend of higher γ' is continued down to the lowest shear rate attainable. The same applies to higher xanthan concentrations, but, beginning at 0.8%, η^* exceeds η, violating the Cox–Merz rule. By 3% xanthan, there is an order of magnitude difference in the two viscosities, though the same power law slope still applies. Cox–Merz violation has previously been reported for xanthan[7,8] and linked to the "weak-gel," easily disrupted nature of the intermolecular interactions over and above entanglement coupling.

During the course of collecting the above creep data, it was noticed that excessively long time periods were required for the viscoelastic components [second term on the right-hand side of eq. (2)] to become dominated by viscous flow. Initially, these long relaxation times were not appreciated and the $J(t)$ curve was interpreted in terms of steady flow when in fact the $J_i\exp(-t/\tau_i)$ terms were still making a contribution. Newtonian plateaus were then found at all concentrations. Only when creep curves were collected over periods of several hours were reliable flow data obtained, leading to the continued shear thinning behavior of Figure 1(a) and (b).

Representative compliance/time curves that demonstrate these long relaxation times are plotted in Figure 6(a) and (b). At the lowest applied stresses possible on our rheometer, the 0.3 and 0.5% samples clearly show a rather rapid (~ 100 s) shift to purely

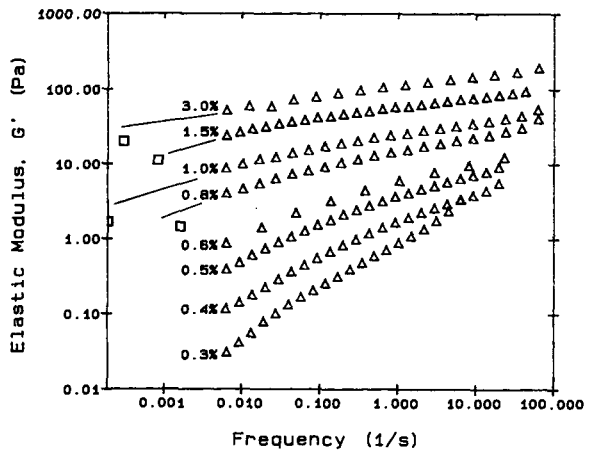

Figure 2 Dependence of the elastic modulus, G', on frequency for varying xanthan concentrations. Square symbols are the shear modulus, G, evaluated as the reciprocal of the limiting compliance (Table I), plotted versus the reciprocal retardation time (Figure 7).

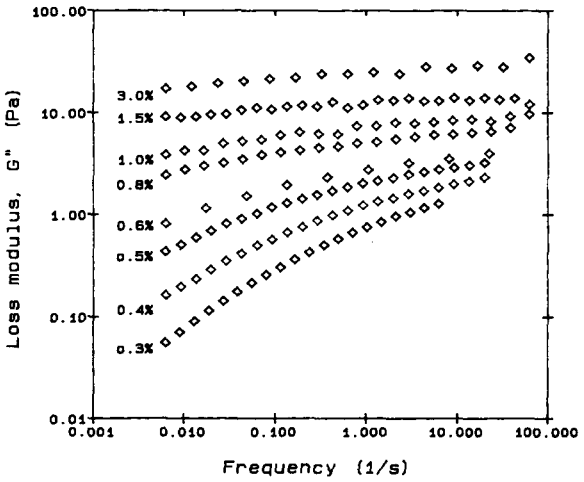

Figure 3 Dependence of the loss modulus, G'', on frequency for a range of xanthan levels.

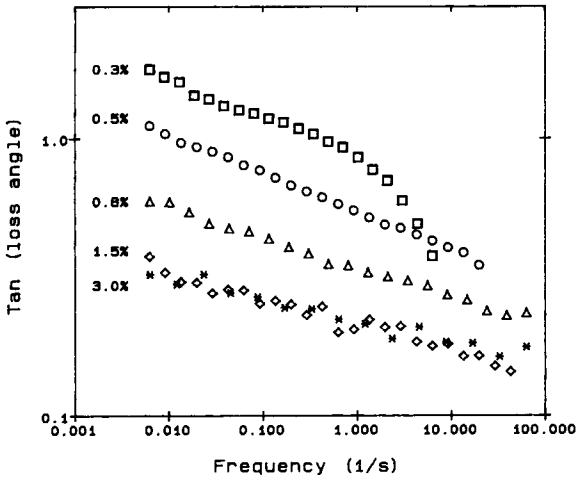

Figure 4 Dependence of tan (loss angle) on frequency over a range in xanthan concentration.

viscous flow, whereas the low stress-limiting behavior of the 1.5 and 3% samples showed a more drawn-out decay of viscoelasticity and also showed a flat $J(t)$ trace for long times. We have interpreted this latter behavior as indicating the existence of a yield stress,[31] which we define simply as a stress below which flow is not observable. This definition is less restrictive than is the conventional one that defines the yield stress as that stress which corresponds to a transition from elastic to plastic deformation.[32] If the shear thinning trend observed in Figure 1(a) and (b) actually continues for one or two decades lower in shear rate, it would give the appearance of a yield stress on experimentally accessible time scales. Since it is impossible to distinguish a conventional yield stress from the above condition, we have applied the first definition and recognize that future advances in instrumentation may force us to alter our interpretation. The abrupt steps in the compliance leading from one plateau to another in the 1.5 and 3% traces will be discussed below. Only xanthan levels of 0.8% and above gave the plateaus in $J(t)$ that indicated a yield stress. However, our instrumental lower limit of 0.08 Pa applied stress may have prevented study of any yield phenomena at lower xanthan concentrations. The value of the compliance in the first plateau, determined over a range of shear stresses, is designated as J_{lim} and is listed in Table I. Also included are the yield stresses, beyond which these plateaus are replaced by steady flow, giving the flow curves of Figure 1(a) and (b).

As an indication of the magnitude of the relaxation times and the way in which they changed with concentration, we have fit creep curves like those in Figure 6(a) and (b) to eq. (2) using the Carri-Med software. The entire curve was used in the fitting procedure for the lower xanthan levels while only the region up to the first plateau was chosen for higher concentrations. At the lowest possible applied stress, the 0.3 and 0.4% samples were already into the regime where the fitted relaxation times depended upon the stress. Thus, the results of the fitting for the 0.3 and 0.4% samples are likely to be underestimates of the relaxation time. However, the true times are unlikely to exceed that of the 0.5% sample that was determined to tend toward a constant value with decreasing stress. At lower concentrations, only one term in the series of J_i was needed, whereas at higher concentrations, two terms were required. Figure 7 demonstrates that the log of the retardation time (τ_i) increases smoothly with the log of concentration, reaching roughly 10,000 s at 1% Xanthan. Beyond this concentration, the longest retardation time remains relatively constant, whereas the second time parameter becomes necessary to fit the data and grows shorter with concentration. Long relaxation times and nonlinear behavior have been reported previously for xanthan systems at high concentrations when studied by step shear rate and stress-relaxation techniques.[7,8,14]

The reciprocal of the J_{lim} values in Table I may be interpreted as the equilibrium shear modulus for these materials. G, defined in this way, is plotted onto Figure 2 using the appropriate reciprocal retardation time of Figure 7 as the frequency. The fact

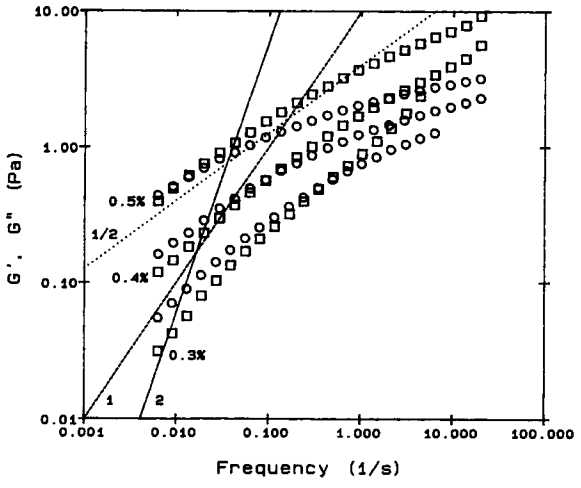

Figure 5 Frequency variation of G' (square symbols) and G'' (circle symbols) for dilute xanthan solutions compared with the predictions of the Rouse model. $G' \sim \omega^2$ (slope = 2) and $G'' \sim \omega$ (slope = 1) in the limit of low frequency for the Rouse model. Similarly, both moduli are predicted to go as $\sqrt{\omega}$ (slope 1/2) in the limit of high frequency.

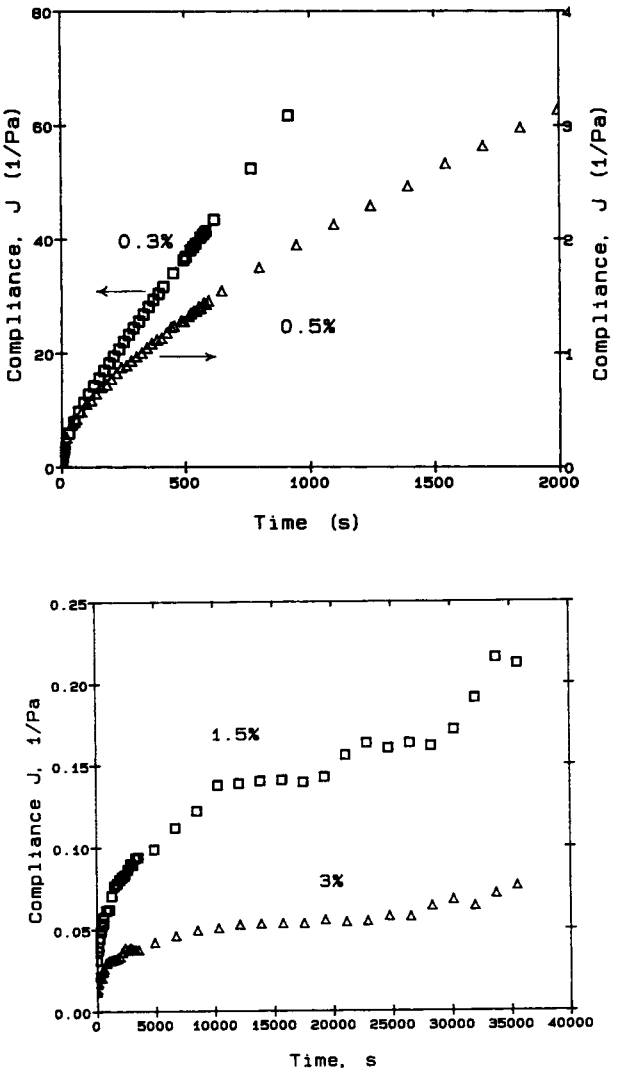

Figure 6 (a) Compliance/time curves for 0.3% and 0.5% xanthan obtained at the lowest reliable applied shear stress. (b) Compliance/time curves for 1.5% and 3% xanthan obtained at shear stresses below the yield stress.

that G from creep data in the preyield region falls below the extrapolated trend in G' indicates that substantial relaxation mechanisms operate at frequencies below the 0.006 s^{-1} limit explored by mechanical spectroscopy. This finding is simply a further indication of the long relaxation times found above.

In light of the high xanthan levels employed in this study, it was thought prudent to examine the samples studied for the presence of optically anisotropic phases. This determination was initially done by holding samples contained in glass bottles in between crossed pieces of polarized film and noting the presence of any birefringence. Although static, permanent birefringence has been reported for xanthan levels of 3% and over,[5,14] we surprisingly saw it using the above simple technique at concentrations $\geq$ 0.8%. Shear-induced birefringence was noticeable upon shaking bottles at any of the xanthan levels used in this study, but such birefringence relaxed quickly (< 1 s) for concentrations under 0.8%. Identical observations were made in samples prepared from the purified xanthan, made from a second batch of Keltol T, or made using other grades of Kelco xanthan. We next sought to confirm our findings using a polarizing microscope with the sample held between the usual microscope slide and cover glass combination. The 3% xanthan sample showed the uniformly dispersed highly birefringent pattern typical of a nematic phase,[33] but lower concentrations appeared isotropic. Only when the cover slide was left off so that thicker samples could be examined were anisotropic textures detected all the way down to 0.8% xanthan. At the lower concentrations, the texture consisted of birefringent patches that resembled those at 3% but which became more widely spaced and thinner as the concentration decreased. The overall impression was that xanthan samples, of concentrations 0.8% and over, consisted of dispersions of anisotropic phase. Attempts to isolate the anisotropic phase by centrifugation (27,000g for 2 h) or by ultrafiltration (0.22 μm filter) were unsuccessful.

Taking a more quantitative approach, a UV/visible spectrophotometer was modified as described in the Experimental section and used to measure the depolarized light intensity from samples at 500 and 600 nm.[34] The results at 500 nm, as a function of

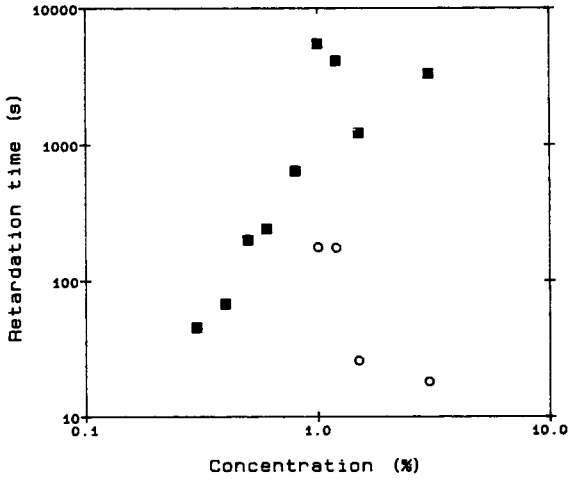

Figure 7 Growth of the long retardation time (square symbols) and the change in the short retardation time (circle symbols) with xanthan concentration.

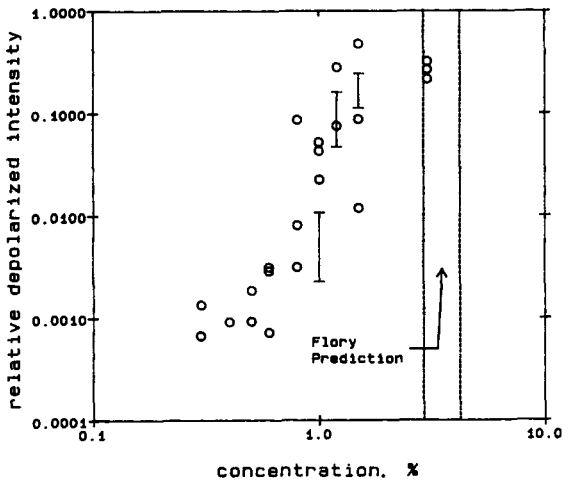

Figure 8 Variation of the depolarized light intensity with the xanthan concentration. The error bars give an estimate of the spatial variation of the depolarization within the sample (see text). The dotted lines indicate the two-phase region predicted by Flory's theory [eqs. (3) and (4)].

concentration, are plotted in Figure 8. The considerable scatter of the data points reflects the heterogeneity described above. Since the illuminating beam was in this case only 2 mm wide, we were able to demonstrate this heterogeneity by making measurements at two different positions within the sample cell—the usual central position and at a spot 8 mm further toward the bottom of the cell. The error bars on Figure 8 reflect the range in depolarized intensity found by the above procedure. Despite the scatter, a trend is quite evident. Significant depolarization occurs for xanthan concentrations in excess of about 0.8%. The scatter in the data disappears by 3%, perhaps indicating that the entire sample is homogeneously anisotropic at this point.

The onset of detectable anistropy and the achievement of a completely anisotropic sample can be used as apparent phase boundaries for the appearance of an anisotropic phase and the disappearance of an isotropic phase, respectively. These phase boundaries can be compared with those predicted by Flory[35,36] for a solution of rod-shaped particles interacting through hard-sphere-type potentials. The driving force for the phase separation is the release of entropy upon leaving the isotropic phase where excluded volume effects severely limit the number of possible configurations for rod-shaped particles. The volume fraction v_2^* at which the anisotropic, nematic phase would first appear in a system of rods with aspect ratio X is given by

$$v_2^* = \frac{8}{X}\left(1 - \frac{2}{X}\right) \tag{3}$$

and the isotropic phase should disappear completely into the anisotropic phase at

$$v_2^A = 11.6/X \tag{4}$$

Estimates appearing in the literature for X vary widely and range to as high as 750.[37-39] This discrepancy is, however, strongly entwined with the structural controversy involving xanthan concerning the number of single chains involved in the helix. It is surely more self-consistent to use our intrinsic viscosity data to estimate the aspect ratio using the well-known Simha relation for a prolate ellipsoid[2,20]:

$$[\eta] = \nu_2 f = \nu_2\left[\frac{14}{15} + \frac{X^2}{15(\ln 2X - 3/2)} + \frac{X^2}{5(\ln 2X - 1/2)}\right] \tag{5}$$

The experimental value for $[\eta]$, 55.7 dL/g, implies an axial ratio of 450 and means that v_2^* should be approximately 0.018 and that v_2^A should be roughly 0.026. With a partial specific volume, ν_2, of 0.62 cm^3/g,[8,20] these estimates translate into concentrations of 2.9% and 4.2%, respectively. These theoretical phase boundaries are drawn in Figure 8. The onset of the anisotropic phase is not predicted to occur until some 3.5 times the concentration at which it is first observed.

DISCUSSION

There seems to be ample evidence, both in this work and in related studies,[6,7,14] to indicate that so-called weak-gel properties show up in xanthan solutions at concentrations in the neighborhood of 0.5%. From this work, we have the following symptoms: (1) onset of deviation from the Cox–Merz rule, (2) appearance of a weak power-law dependence of G' and G'' on frequency, (3) appearance of a long-time relaxation mode, and (4) evidence for an apparent yield stress. There is also the unabated shear thinning of η that is atypical of a polymer solution. The most interesting aspect of this study is the appearance of an anisotropic phase at xanthan concentrations in close proximity to the onset of these weak-gel properties. The anisotropic phase is identified by a static, permanent birefringence. Our micro-

scopic evidence indicates that this anisotropic phase is present as a dispersion and that its volume fraction increases with polymer concentration in the usual way.

Despite the fact that the above gel symptoms are usually linked to weak noncovalent interactions acting between individual xanthan molecules,[8] we are led to the inevitable conclusion that the cause of the unusual rheology of xanthan is, for this case at least, the presence of interacting domains of dispersed, anisotropic phase. Ample evidence exists for the formation of such domains in xanthan.[14,40] At high concentrations, these domains display the textures characteristic of cholesteric liquid crystal phases,[41,42] and the rheology of such systems shows many of the symptoms that we have observed.[43-45] In particular, we see rheological behavior typical of Region I flow behavior in Wissbrun's classification.[46] This region is characterized by strong shear thinning at low shear rates, long-time effects such as thixotropy, and long relaxation times and an apparent yield stress.

Strong evidence for a heterogeneous nature to concentrated xanthan samples comes from creep runs of 3–10 h duration. Such a run, on 1.5% xanthan, is shown in Figure 6(b). The compliance/time presentation is marked by the appearance of several plateaus: portions of constant compliance separated by sudden jumps to a higher constant level. This behavior was seen at low stresses for all xanthan concentrations over 0.8% but gradually disappeared at higher stresses, leaving a smoothly varying compliance curve. We have interpreted these plateaus as indicating metastable yield points due to the network formed by the dispersed phase. Evidently, this network reorients very slowly under stress and finds new equilibrium positions to which it shifts rather suddenly, accounting for the jumps in compliance.

The relaxation times of Figure 7 provide further evidence of some sort of phase-separation explanation. The plateau in the longest relaxation time beginning at about 1% xanthan suggests the presence of domains whose local polymer concentration is insensitive to the bulk polymer level.[47] The volume fraction of such domains would increase with the bulk polymer level, but since the local environment inside each domain would remain unchanged, the relaxation phenomena would be expected to likewise remain the same. What was found to be surprising was the variation of the relaxation-time distribution with concentration. The fraction of the total compliance (J_1/J) that is due to the long relaxation time remains approximately constant at 0.6 ± 0.1 over the range 0.8–3%. It would seem that the relative contribution of J_1 should be expected to increase with concentration in a phase-separation model.

Lastly, recent work by Allain et al.[48] on the viscosity and optical properties of xanthan has also detected anisotropic phase formation at low polymer concentration (0.7 wt %). These workers further observed the occurrence of a maximum in the viscosity as a function of xanthan concentration at a concentration of 6.5%. This maximum is a classical symptom[46] that an anisotropic phase is present.

A question that still remains is that of whether the anisotropic phase is simply a manifestation of the microgel or is more akin to the phases formed by some polyamides, polyesters, and other rodlike polymers.[49] The phase diagram comparisons of the earlier section show that the anisotropic phase appears earlier than was predicted by the Flory[35] theory for hard rods. Various explanations can be put forth to explain this difference. We have considered (1) use of an inappropriate model for the rod thermodynamics, (2) polydispersity, and (3) polymer–polymer attractive interactions.

The Flory theory predicts that anisotropic-phase formation should occur at a polymer concentration of 2.9% instead of the 0.8% observed. There have been, of course, other estimations of the concentration at which rigid rods will form an anisotropic phase. Onsager[50] first treated the problem of a rodlike gas and used a virial expansion, truncated at the second term, to predict, in the current notation, the onset of anisotropic phase formation at

$$v_2^* = 3.34/X \tag{6}$$

The exclusion of higher-order terms in the virial expansion leaves this approach lacking at higher concentrations. The lattice approach due to Flory[35] lifted, somewhat, this concentration restriction by estimating the number of ways in which the rods can be assigned with discrete orientations to the lattice. The two approaches do not agree, however, at large X, which should correspond to the dilute rod limit. Further extensions of Flory's treatment by DiMarzio,[51] who allowed for a continuous distribution of rod orientations, and by Flory and Ronca,[52] who made a more exact lattice calculation, have resulted in only very minor alterations to the predictions of eq. (3). A recent approach based on caging phenomena[53] has suggested the onset of order at significantly lower concentrations but has not been verified in terms of macroscopic anisotropy.

Sticking with the Onsager estimate of v_2^*, we could justify the anisotropic phase appearing at concentrations over 1.2 wt %. Polydispersity in the xanthan rod length could then be responsible for a further reduction in the predicted v_2^*. Flory[54] has argued that the aspect ratio calculated from the weight-average molecular weight is the appropriate way to handle polydispersity. Since we based our calculations on the viscosity average molecular weight, significant polydispersity ($M_w/M_v \sim 1.5$) would explain our findings. M_w/M_n for xanthans has been reported in the range 1.2–2,[12,38,39,55] with occasionally higher values being noted.[56] Although M_v used here is closer to M_w than is M_n, this line of reasoning could still be plausible.

In addition to the above explanation based on hard rod packing combined with polydispersity, attractive interpolymer interactions might also be responsible for the low observed value of v_2^*. In Flory's original treatment,[35] polymer/solvent interactions were included via the familiar interaction parameter χ. Isotropic, endothermic rod/solvent mixing would hasten anisotropic phase separation. A sensitive indication of this kind of interaction is the second virial coefficient that should be diminished below the hard rod limit in the case of attractive interactions. Experimental determinations of A_2 from light scattering[12,39,55] have produced values on the order of 5×10^{-4} cm^3 mol/g^2. These values agree well with estimates made using the theoretical hard sphere limit for a rigid rod having the same diameter d and mass per unit length M_l as xanthan. Using[57]

$$A_2 = \pi N_A d/4M_l^2 \qquad (7)$$

and the range of values mentioned above, the resulting estimates fall in the range $2\text{–}10 \times 10^{-4}$ cm^3 mol/g^2. Thus, the experimental A_2 values can be justified, making any explanation based on isotropic, endothermic mixing seem improbable.

However, orientationally dependent interactions cannot be directly ruled out.[35] Some types of intermolecular interactions can be dependent on the relative orientation of the molecules. An example are dispersion forces that are due to the orientationally dependent polarizabilities of certain groups on the polymer chain.[54] For these cases, the free energy of the system can be lowered by molecular alignment. In the case of xanthan, orientationally dependent interactions could include hydrogen bonding or the hydrophobic interactions between pyruvate substituents on the periphery of the helix.[10] Evidence that forces of this type are present in xanthan are rather convincing and include all the evidence for association of xanthan chains mentioned earlier.[9,14,37] In addition, light scattering has shown that the molecular weight of the xanthan helix increases strongly with the ionic strength in the range 0.01–0.1N,[37,38,58] whereas the radius of gyration increases more weakly.[9] These observations suggest side-by-side association of the chains as do intrinsic viscosity studies,[15,37,38] which are consistent with four or more single strands per helix.

To get an estimate of the magnitude of the anisotropic interactions that would be necessary to explain the observed v_2^*, use was made of the extensions by Flory and Ronca[59] and by Warner and Flory[60] on the original Flory theory. In this generalized approach, the extra-attractive energy operative for optimally aligned chain segments is expressed as kT^* per segment.[54] As T^* increases from zero, v_2^* is seen to at first decrease slowly. Then, just beyond a critical value of the anisotropic interaction, the phase equilibria include either the usual isotropic/anisotropic pair or a pair of anisotropic phases. As T^* is increased further, a triple point is reached past which v_2^* decreases more rapidly and v_2^A becomes large, leading to a very wide biphasic region. In the application of the scheme proposed by Warner and Flory[60] (see the Appendix for details) to the problem of $X = 450$, the anisotropic interactions were turned on by increasing T^* until the calculated v_2^* matched the experimental value. The estimated energy was found to be 0.079 kT. Taking this value as the order of magnitude of the orientationally dependent force, it seems not at all unlikely that hydrophobic forces ($\sim$ 2 kT per CH_2 group) or hydrogen-bonding forces (7.6 kT per hydrogen bond) could have an anisotropic component of the above magnitude. For the hydrophobic case, one might envision a reduced surface area for hydrophobic groups arising from more efficient packing of parallel rods as the anisotropic mechanism.

The strength of interaction found above places our system in the wide biphasic region of the phase diagram ($v_2^A = 0.94$). Although our own estimate of v_2^A from depolarization data is rather approximate, Allain et al.[48] have put it at 0.053. We could blame the deviation from theory on polydispersity or on the fact that xanthan forms a cholesteric rather than nematic phase at high concentrations. However, it seems more likely that neither the hard rod nor the current anisotropic interactions models are entirely appropriate for the system at hand. Some refined theory, perhaps also including polydispersity ex-

plicitly and with different statistics for the ordered phase, would probably be necessary. Specific cation-mediated interactions may also be contributing factors. To test such a theory would require more data than we presently have available, and the formalism would almost certainly still contain anisotropic interactions as an important facet. We have taken the extreme case of assigning all deviations from the early Flory theory to these interactions and find that the energies involved are entirely reasonable.

Justification of the appearance of the anisotropic phase in terms of the above existing principles thus seems possible, and we are in agreement in this regard with Allain et al.[48] As regards the relative importance of, and connection with, microgels, these matters were investigated experimentally, using the fact that several reports[9,15,61] have recommended heating xanthan solutions to temperatures as high as 80–90°C (well above the helix-to-coil transition in the absence of salt) as a way to get reduced microgel content upon cooling. This effect of temperature on anisotropy was studied in detail by sealing samples with xanthan concentrations spanning the range 0.4–2% in glass ampules and then thermostating them over the temperature range 15–85°C. As Figure 9 indicates, the xanthan concentration marking the transition between transient and permanent birefringence moved gradually to higher levels with temperature but then jumped suddenly at 85°C, leaving all the samples isotropic. Presumably, this result is due to the denaturation of the xanthan coil that is expected to occur at about 85°C for the prevailing ionic strength.[27] The denatured

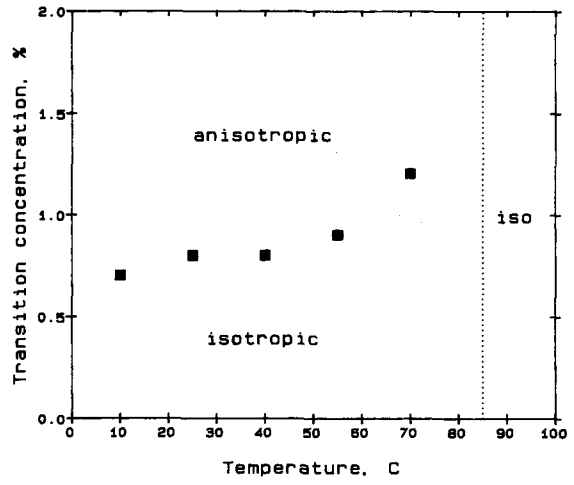

Figure 9 The change in the concentration of xanthan at which the anisotropic phase first appears as a function of temperature.

polymer loses some of its rigidity and so no longer has the high aspect ratio required for anisotropic phase formation. Upon cooling to room temperature, birefringence returns spontaneously for xanthan concentrations of over 0.8%, even in the absence of shear, and shear-induced birefringence is again permanent down to 0.8% xanthan. The same result was obtained with a 1.5% solution that was autoclaved (121°C, 25 min) and then subjected to ultrafiltration (0.22 μm pore size). These steps should have ensured that a true xanthan solution was obtained, yet optical anisotropy was again evident immediately upon cooling the sample. These results, particularly the spontaneous return of birefringence, strongly suggest that these phenomena are not related to traditional microgels.

CONCLUSIONS

Xanthan gum is found to form a "weak gel" in 0.02*N* KCl at concentrations exceeding 0.8%. The characteristics of this gel are in all ways identical to those found in similar studies and include significant nonlinear and thixotropic behavior and deviations from the Cox–Merz rule. In addition, we have used creep measurements to detect the presence of a yield stress that first appears at the aforementioned concentration. Further, a plateau in the concentration variation of long relaxation times measured during creep and the discontinuities in the creep curves themselves suggest that the structure of these gels is heterogeneous. This supposition is confirmed by a variety of optical studies that indicate that an anisotropic phase first occurs at around the 0.8% level and exists as a dispersion within an isotropic phase.

The fact that this phase occurs spontaneously above a certain concentration combined with its anisotropic optical properties rules out any connection with the microgels commonly reported in xanthan solutions. However, the predictions of Flory's lattice theory clearly overestimate the xanthan concentration for the appearance of the ordered phase. The irrefutability of the experimental data must then indicate the presence of an aggravating factor that favors the separation of the anisotropic phase. One such factor may be polydispersity, and a second could be attractive interactions, over and above those of hard rods, acting between xanthan molecules. The latter supposition is shown to be quite plausible based on a simple calculation. Thus, the unique rheological properties of xanthan gum appear to be due to its equally unique solution properties.

I would like to acknowledge the invaluable assistance of R. Oseredczuk with sample preparation and rheological experimentation and of M. Naser with the intrinsic viscosity measurements. S. B. Ross-Murphy is sincerely thanked for his help and encouragement throughout the course of this work. I am grateful to Unilever Research for permitting the publication of these results.

REFERENCES

1. A. Jeanes, J. E. Pittsley, and F. R. Senti, *J. Appl. Polym. Sci.*, **5**, 519 (1961).
2. P. J. Whitcomb and C. W. Macosko, *J. Rheol.*, **22**, 493 (1978).
3. J. G. Westra, *Macromolecules*, **22**, 367 (1989).
4. D. J. Sikkema and H. Janssen, *Macromolecules*, **22**, 364 (1989).
5. J. C. Salamone, S. B. Clough, A. B. Salamone, K. I. G. Reid, and D. E. Jamison, *Soc. Pet. Eng. J.*, **22**, 555 (1982).
6. S. A. Frangou, E. R. Morris, D. A. Rees, R. K. Richardson, and S. B. Ross-Murphy, *J. Polym. Sci. Polym. Lett. Ed.*, **20**, 531 (1982).
7. W. E. Rocherfort and S. Middleman, *J. Rheol.*, **31**(4), 337 (1987).
8. R. K. Richardson and S. B. Ross-Murphy, *Int. J. Biol. Macromol.*, **9**, 257 (1987).
9. V. J. Morris, D. Franklin, and K. I'Anson, *Carbohydr. Res.*, **121**, 13 (1983).
10. I. H. Smith, K. C. Symes, C. J. Lawson, and E. R. Morris, *Int. J. Biol. Macromol.*, **3**, 129 (1981).
11. S. B. Ross-Murphy, private communication.
12. B. Tinland and M. Rinaudo, *Macromolecules*, **22**, 1863 (1989).
13. S. B. Ross-Murphy, V. J. Morris, and E. R. Morris, *Faraday Symp. Chem. Soc.*, **18**, 115 (1983).
14. T. Lim, J. T. Uhl, and R. K. Prud'homme, *J. Rheol.*, **28**, 367 (1984).
15. T. Kojima and G. C. Berry, *Polymer*, **29**, 12 (1988).
16. J. L. Zatz and S. Knapp, *J. Pharm. Sci.*, **73**(4), 468 (1984).
17. M. Milas, M. Rinaudo, and B. Tinland, *Polym. Bull.*, **14**, 157 (1985).
18. J. D. Ferry, *Viscoelastic Properties of Polymers*, Wiley, New York, 1980.
19. M. M. Santore and R. K. Prud'homme, *Carbohydr. Polym.*, **12**, 329 (1990).
20. G. Chauveteau, *J. Rheol.*, **26**, 111 (1982).
21. P. G. deGennes, *Scaling Concepts in Polymer Physics*, Cornell University Press, Ithaca, NY, 1979.
22. G. J. Besio, I. M. Leavesley, R. K. Prud'homme, and R. Farinato, *J. Appl. Polym. Sci.*, **33**, 825 (1987).
23. J. G. Southwick, H. Lee, A. M. Jamieson, and J. Blackwell, *Carbohydr. Res.*, **84**, 287 (1980).
24. H. H. Winter, *Progr. Colloid Polym. Sci.*, **75**, 104 (1987).
25. K. Te Nijenhuis and H. H. Winter, *Macromolecules*, **22**, 411 (1989).
26. P. J. Flory and J. E. Osterheld, *J. Phys. Chem.*, **58**(7), 653 (1954).
27. G. Holzwarth, *Biochemistry*, **15**(19), 4333 (1976).
28. H. W. Bewersdorff and R. P. Singh, *Rheol. Acta*, **27**, 617 (1988).
29. M. Balaban, A. R. Carrillo, and J. L. Kokini, *J. Texture Stud.*, **19**, 171 (1988).
30. N. Gladwell, R. R. Rahalkar, and P. Richmond, *Rheol. Acta*, **25**, 55 (1986).
31. H. A. Barnes and K. Walters, *Rheol. Acta*, **24**, 323 (1985).
32. H. A. Barnes, J. F. Hutton, and K. Walters, *An Introduction to Rheology*, Elsevier, Amsterdam, 1989.
33. K.-S. Yang, M. H. Theil, and J. A. Cuculo, in *Polymer Association Structures—Microemulsions and Liquid Crystals*, M. A. El-Nokaly, Ed., ACS Symposium Series 384, American Chemical Society, Washington DC, 1989.
34. C. K. Ober, J. I. Jin, and R. W. Lenz, *Adv. Polym. Sci. (Liq. Cryst. Polym.)*, **59**, 103 (1984).
35. P. J. Flory, *Proc. R. Soc. A*, **234**(1196), 73 (1956).
36. J. Hermans, Jr., *J. Colloid Sci.*, **17**, 638 (1962).
37. J. G. Southwick, A. M. Jamieson, and J. Blackwell, *J. Appl. Polym. Sci. Appl. Polym. Symp.*, **37**, 385 (1983).
38. A. M. Jamieson, J. G. Southwick, and J. Blackwell, *J. Polym. Sci. Polym. Phys. Ed.*, **20**, 1513 (1982).
39. T. Coviello, K. Kajiwara, W. Burchard, M. Dentini, and V. Crescenzi, *Macromolecules*, **19**, 2826 (1986).
40. G. Maret, M. Milas, and M. Rinaudo, *Polym. Bull.*, **4**, 291 (1981).
41. F. Livolant, *J. Phys.*, **47**, 1605 (1986).
42. F. Livolant and Y. Bouligand, *Mol. Cryst. Liq. Cryst.*, **166**, 91 (1989).
43. K. F. Wissbrun and A. C. Griffin, *J. Polym. Sci. Polym. Phys. Ed.*, **20**, 1835 (1982).
44. B. Erman, I. Bahar, and P. Navard, *Macromolecules*, **22**, 358 (1989).
45. C. Balbi, E. Bianchi, A. Tealdi, and W. R. Krigbaum, *J. Polym. Sci. Polym. Phys. Ed.*, **18**, 2037 (1980).
46. K. F. Wissbrun, *J. Rheol.*, **25**, 619 (1981).
47. E. E. Braudo, I. G. Plashchina, and V. B. Tolstoguzov, *Carbohydr. Polym.*, **4**, 23 (1984).
48. C. Allain, J. Lecourtier, and G. Chauveteau, *Rheol. Acta*, **27**, 225 (1988).
49. T. Itou and A. Teramoto, *Macromolecules*, **21**, 2225 (1988).
50. L. Onsager, *Ann. N.Y. Acad. Sci.*, **51**, 627 (1949).
51. E. A. DiMarzio, *J. Chem. Phys.*, **35**(2), 658 (1961).
52. P. J. Flory and G. Ronca, *Mol. Cryst. Liq. Crys.*, **54**, 289 (1979).
53. G. T. Keep and R. Pecora, *Macromolecules*, **21**, 817 (1988).
54. P. J. Flory, *Adv. Polym. Sci.*, **59**, 1 (1984).
55. T. Coviello, W. Burchard, M. Dentini, and V. Crescenzi, *Macromolecules*, **20**, 1102 (1987).

56. G. Holzwarth, *Carbohydr. Res.*, **66,** 173 (1978).
57. H. Yamakawa, *Modern Theory of Polymer Solutions,* Harper & Row, New York, 1971.
58. L. S. Hacche, G. E. Washington, and D. A. Brent, *Macromolecules,* **20,** 2179 (1987).
59. P. J. Flory and G. Ronca, *Mol. Cryst. Liq. Cryst.*, **54,** 311 (1979).
60. M. Warner and P. J. Flory, *J. Chem. Phys.*, **73**(12), 6327 (1980).
61. J. G. Southwick, M. E. McDonnell, A. M. Jamieson, and J. Blackwell, *Macromolecules,* **12,** 305 (1979).

APPENDIX

The calculation of v_2^* and v_2^A as a function of T^* and X was made following Warner and Flory.[60] The condition of chemical equilibrium requires that the chemical potential of the solvent (water) be the same in the isotropic and anisotropic phases and that a similar equality apply to the chemical potential of the rods (xanthan). For rods of aspect ratio X, we then have

$$(\mu_{solv} - \mu^0_{solv})_{aniso} = (\mu_{solv} - \mu^0_{solv})_{iso} \quad (A.1)$$

$$(\mu_X - \mu^0_X)_{aniso} = (\mu_X - \mu^0_X)_{iso} \quad (A.2)$$

Expressions for both sides of eqs. (A.1) and (A.2) are provided as eqs. (18)–(21) of Ref. 60. Additional self-consistency relationships are also provided for the bulk and local orderings of the rods in the anisotropic phase. Simultaneous solution of eqs. (A.1) and (A.2) yields values of v_2^* and v_2^A as functions of X and T^*. The T^* necessary to give the sought-after v_2^* is found to place the xanthan system well into the biphasic region. This result is in line with those of Warner and Flory who found that the above region emerges at 0.26 kT for $X = 50$ and appears at decreasing T^* with increasing X. Apparently, this trend is due to the increased number of favorable contacts possible for rods of large X.

Received May 21, 1990
Accepted December 6, 1990